INVESTIGATION OF CRACK PROPAGATION PROPERTIES OF ADDITIVE MANUFACTURING PRODUCTS

H. Abramovich*, N. Broitman, A. Shirizly****
* Faculty of Aerospace Engineering, Technion, I.I.T., 32000 Haifa, Israel,
** Faculty of Mechanical Engineering, Technion, I.I.T., 32000 Haifa, Israel

Keywords: *additive manufacturing, crack propagation, selective laser melting, Ti-6Al-4V specimens, thermal treatment*

Abstract

The present study focuses on a process called SLS (Selective Laser Sintering) which applies for metal parts. As the additive manufacturing method is still in its initial steps the structural integrity of its products must be examined and compared to other typical processes. Therefore, the present study investigates the crack propagation properties of Ti-6Al-4V which has been manufactured by selective laser sintering and in comparison, to cold rolled Ti-6Al-4V samples. The results include crack propagation behavior of Ti-6Al-4V manufactured by SLM in a few directions of the manufacturing method, as well as, a few thermal treatments which the samples had been processed through. It was found that the crack propagation properties of SLM produced specimens are similar to cold rolled specimens.

Making use of one of the biggest advantages of additive manufacturing method, namely, its ability to create with the same effort a very complex geometry which in some cases is impossible to create by other manufacturing methods, two lattice structures had been suggested, with one of them having a better crack propagation resistance.

1 Introduction

Engineers uses well known manufacturing technologies. Each technology has its strengths and its weak sides and the designer usually takes all of them into his considerations during the design process. To be able to perform his task, the designer has to know all the structural and material properties after being processed by the selected technology including strength, Young's and shear modulus, fatigue properties or crack propagation properties including critical stress intensity factor. The strength and Young's modulus can be found by performing a standard tensile test [1]. The stress intensity factor is used to predict the stress state ("stress intensity") near the tip of a crack caused by a remote load or residual stresses. The stress intensity factor is influenced by the surrounding stress field, the general geometry of the specific structure and the crack length. To determine the value of a stress intensity factor at failure, material critical stress intensity factors ($K_{I_c}, K_{II_c}, K_{III_c}$) [2, 3] must be known. For instance, the K_{I_c} value of a material can be determined by performing a standard stress intensity factor test [4].

Fatigue can be evaluated in two ways. The first one is by using the well-known S-N curve which is based on a series of tests being performed on a specimen. On each test, a load which is lower than the predicted failure load is cyclically, applied until the failure of the specimen. At failure, the number of cycles which has been applied is recorded and after a series of tests a curve of stress versus the number of cycles is being generated. This curve is used to predict the life cycle of a structure under cyclic loads. The S-N characterization can be performed using a standard ASTM method [5]. The second way is to characterize the crack propagation by applying a cyclic load on a standard specimen having a pre-determined crack and measuring its length during the test as a function of the number of cycles. This method gives a material unique graph by linking between the stress intensity factor and the crack propagation rate. The crack propagation characterization is done using a standard ASTM method [6].

Additive manufacturing is a process in which a solid geometry is being built by adding material in powder form, melted either by laser of electron beam. Some patents presenting the technology can be found in [7, 8 and 9]. The additive manufacturing (AM) technology, sometimes also called 3D printing, is a relatively young technology. This technology introduces a wide range of geometrical opportunities which were almost impossible to manufacture by other technologies as well as manufacturing time durations which were significantly reduced.

Relatively, only a few studies on additive manufacturing products have been published in the literature. These include, the evaluation of the strength of titanium alloys [10, 11, 12], studies on fracture toughness presenting K_{I_c} values [11], the realization of the S-N curve [13] and crack propagation tests [13,26]. Those studies can be considered as initial studies and this field requires further research in order to give enough confidence in the mechanical properties obtained after the additive manufacturing processing.

In view of what has been described above, the present research aims at enlarging the material data base, by focusing on the crack propagation of Ti-6Al-4V manufactured by AM using the direct laser melting process in comparison to Ti-6Al-4V machined from cold rolled ¾" plates. The tested samples included machined cold rolled ¾" plates which were stress relieved, AM samples in two directions (along the manufacturing plane and perpendicular to manufacturing plane) with some of the specimens being stress relieved and some after undergoing a HIP heat treatment. After characterizing the crack propagation of solid materials for the above-mentioned configurations, novel lattice structures were examined.

As mentioned above, AM technology opens opportunities to manufacture very complex geometries with the same effort of manufacturing a simple one. One of the complex structures is a lattice structure. The present study evaluated two configurations of lattice structures: The first one is named *Poles Structure*. This structure has 3 perpendicular directions intersect poles. The second configuration, called the *Pits Structure* has 3 perpendicular directions of intersect pits surrounded by solid material.

2 Experimental Procedures

2.1 Specimens manufacturing

The geometry of the samples is according to ASTM E399 [4] with the variables w and B (Figure 1) being W=1" (25.4mm) and B=½" (12.7mm).

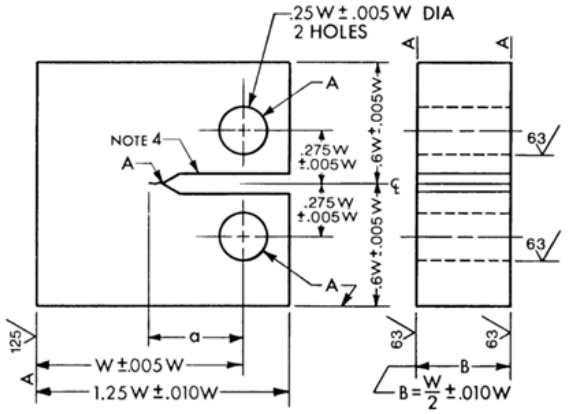

Fig. 1 Schematic Drawing of the Crack Propagation Specimen

The reference samples were machined from cold rolled ¾" plates which were stress relieved before machining, while the AM ones were produced by EOS M280, 200 Watt laser machine using a metal powder with grain having a typical diameter of 20 [µm] in an argon environment chamber. The samples were manufactured oversized and machined after manufacturing. The manufacturing directions are defined in Figure 2.

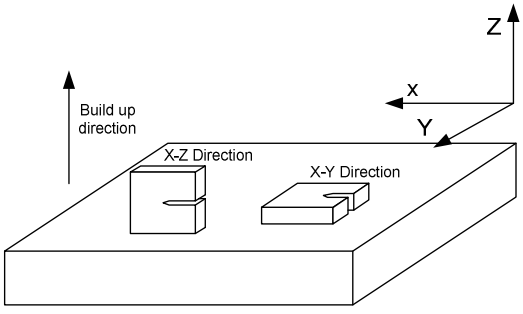

Fig. 2 AM Samples Production Directions

The third type of samples, the lattice samples, were produced to their final geometry by EOS, 200 W laser machine using metal powder with typical grain diameter of 30 [μm]. The manufacturing process was followed by a stress relief heat treatment. The two configurations of lattice structures are:

a. Poles structure

This lattice structure (Figure 3) is combination of 0.7 [mm] diameter poles in 3 perpendicular directions, at 45º offset from two major coordinates of the specimen. The distance between the centers of two adjacent poles is 1.5 [mm] yielding 37.5% volume fracture.

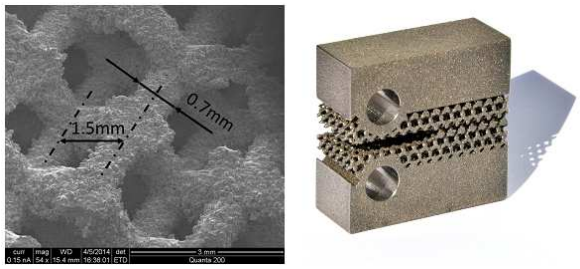

Fig. 3 Poles Type Lattice Structure

b. Pits structure

This lattice structure (Figure 4) is a combination of 1 [mm] diameter pits in 3 perpendicular directions, at 45º offset from two major coordinates of the specimen. The distance between the centers of two adjacent poles is 1.5 [mm] and thus obtaining a structure volume fracture of 37.5%.

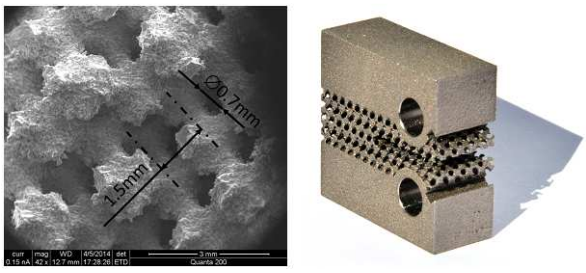

Fig. 4 Pitts Type Lattice Structure

Note that the sharp corners obtained at the poles intersections will cause stress concentrations which might lead to a faster failure in comparison with the pits structure which has no sharp corners.

Two types of heat treatments were applied on some samples: the first one, the stress relief, included hot soaking of the specimen at 650ºC for 3 hours, while the second one, the hot isostatic pressure (HIP) consisted of hot soaking of the specimen at 925ºC in a high-pressure chamber (approx. 96.6 MPa) for 3 hours.

2.2 Test Setup

The tests were performed on a MTS hydraulic fatigue tensile machine equipped with a 100 [kN] load cell. At the end of the crack, a MTS COD (crack opening displacement) gage was placed and it measured the crack opening value at each load cycle (Figure 5). For tests on solid specimens, a crack length gage Vishay TK-09-CPA01-005/DP was bonded to the specimen (Figure 6). The gage has 20 wires at 0.25 [mm] distance between two adjacent ones and as the crack propagates the wires tear thus indicating the crack length.

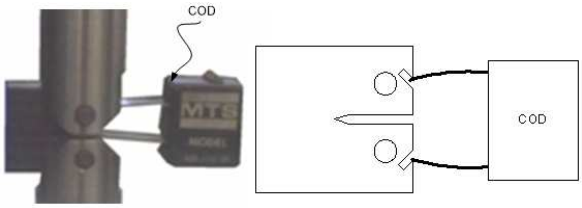

Fig. 5 COD Implementation

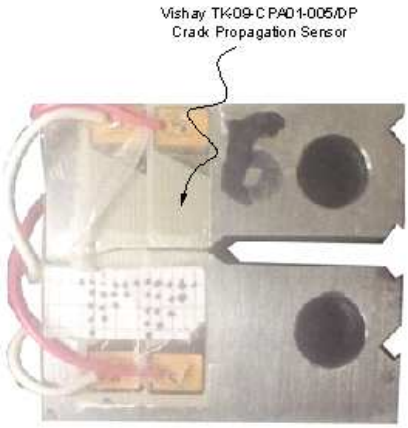

Fig. 6 Crack Propagation Sensor Implementation

2.3 Test Procedure

The sample was installed on the loading machine which applied a 10 [Hz] sinusoidal load

at R=0.1 (i.e. the machine applies only tensile force). During the test, every 10 cycles, a sample of the crack length gage and a sample of the COD gage were taken and stored. The various performed tests are summarized in Table 1. The output measurements include the maximum and minimum force at each cycle and the amplitude of the COD gage and the readings of the crack propagation sensor. The large data base is then filtered to reduce its size for further processing, by keeping only the data when the crack length changes its value by 1.

Table 1 Test Matrix

No.	Name	Prod. Method	Sample	Dir.	T.T.*	Test
1	Cr1	C.R.**, machined	Solid	CPR[!]	S.R.[@]	CP[&]
2	Cr2	C.R., machined	Solid	CAR[$]	S.R.	CP
3	Cr3	C.R., machined	Solid	CPR	S.R.	CP
4	Cr4	C.R., machined	Solid	CAR	S.R.	CP
5	Cr5	C.R., machined	Solid	CPR	S.R.	CP
6	AM1	AM	Solid	X-Y	S.R.	CP
7	AM2	AM	Solid	X-Y	S.R.	CP
8	AM3	AM	Solid	X-Y	S.R.	CP
9	AM4	AM	Solid	X-Y	S.R.	CP
10	AM5	AM	Solid	X-Y	S.R.	CP
11	AM6	AM	Solid	X-Y	S.R.	CP
12	AM7	AM	Solid	X-Z	S.R.	CP
13	AM8	AM	Solid	X-Z	S.R.	CP
14	AM9	AM	Solid	X-Y	HIP	CP
15	AM10	AM	Solid	X-Y	HIP	CP
16	AM11	AM	Poles	X-Y	S.R.	CP
17	AM12	AM	Poles	X-Y	S.R.	CP
18	AM13	AM	Pits	X-Y	S.R.	CP
19	AM14	AM	Pits	X-Y	S.R.	CP

*T.T. =Thermal Treatment, **C.R.=Cold Rolled ,[!]CPR= Crack perpendicular to rolling; [@]S.R.=Stress Relieved, [$]CAR= Crack along rolling; [&]CP= Crack propagation

For each cycle the stiffness of the tested specimen is using the following relation:

$$k_s = \frac{Force_{\max} - Force_{\min}}{COD_{length}} \qquad (1)$$

After calculating the stiffness of the specimen with respect to the crack length, a polynomial expression is curve fitted between the crack length and the stiffness defined in Equation 1. A typical graph of the crack length vs. the specimen's stiffness is presented in Figure 7.

Knowing the crack length and the applied load yields the ΔK_1 values for the entire data as well as the crack length rate da/dN (a is the crack length and N stands for the number of cycles) leading to a graph of the crack length rate vs. ΔK_1 (Figure 8). ΔK_1 is calculated using the following expression

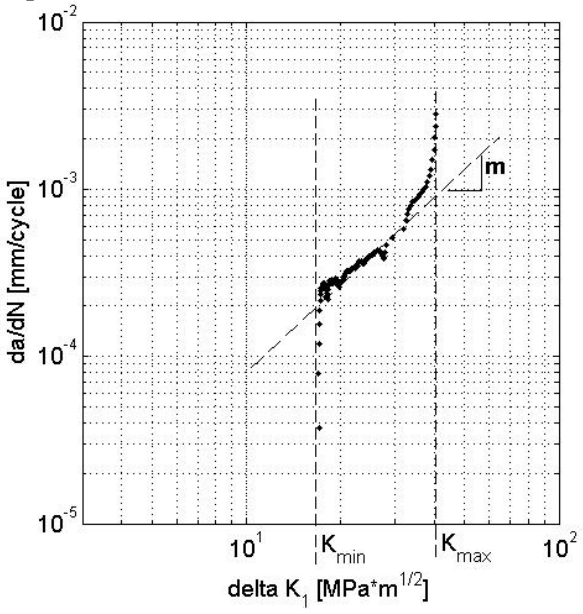

Fig. 7 Typical Graph: Crack Length (a) vs. Specimen's Stiffness (k) - A

$$\Delta K_1 = \frac{\Delta P}{B \cdot \sqrt{W}} \cdot f\left(\frac{a}{W}\right) \qquad (2)$$

where

$$f(\chi) = \frac{2+\chi}{(1-\chi)^{\frac{3}{2}}}\Gamma,$$

$$\Gamma \equiv \left[0.886 + 4.64(\chi) - 13.32(\chi)^2 + 14.72(\chi)^3 - 5.6(\chi)^4\right]; \qquad (3)$$

$$\chi \equiv \frac{a}{W}.$$

ΔP is the load amplitude, a is the crack length W and B are the dimensions as presented in Figure 1.

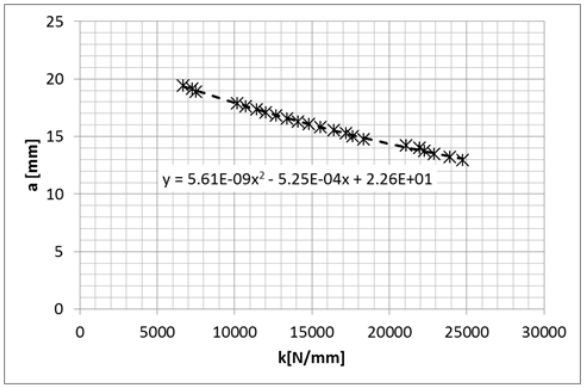

Fig. 8 Typical Graph: (da/dN) vs.ΔK_1

The graph depicted in Figure 8 enables to find the Paris coefficients C and α appearing in Paris law [23,24] as expressed by the following equation

$$\frac{da}{dN} = C \cdot \Delta K^{\alpha} \qquad (4)$$

where

$$\Delta K = K_{\max} - K_{\min} \qquad (5)$$

One should note that for the typical graph shown in Figure 8, the following values were obtained : $\alpha = 1.86$, $K_{\min} = 17\left[MPa \cdot \sqrt{m}\right]$, $K_{\max} = 40\left[MPa \cdot \sqrt{m}\right]$ and $C = 6.92 \cdot 10^{-21}\left[m^{0.5} / (cycle \cdot MPa)\right]$.

When $da/dN \to \infty$, $K_{\max} \to K_{1C}$ and sometimes $K_{\min}$ is also named ΔK_{th}, occurred at lower threshold value of da/dN, below which no crack propagation would occur.

2.4 Results

The results for the five cold rolled samples are presented in Figure 9, which displays the crack length rate vs. ΔK_I and summarized in Table 2. In addition, microscope photos of the cold rolled specimens were taken to compare their crack surface properties to those belonging to specimens produced by the AM technique.

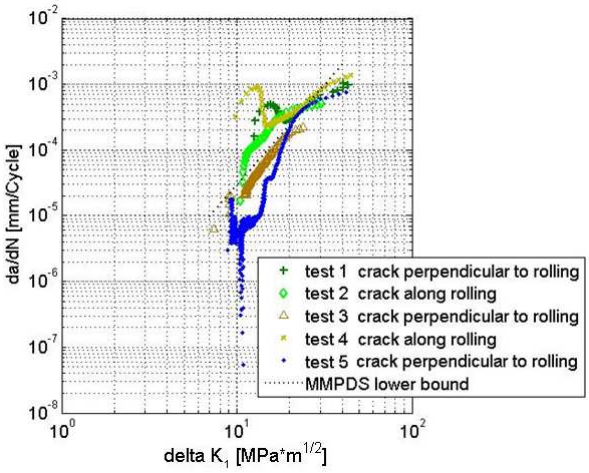

Fig. 9 Five Cold Rolled Specimens Results

It seems that the results are in close agreement with the results presented in the Metallic Materials Properties Development and Standardization Scientific Report (MMPDS) [25]. Moreover, the microscope photos reveal a micro-structure resembling micro-structure of cold rolled Ti-6Al-4V material, a surface typical to a fatigue crack appearing at the fatigue area and a surface typical to a crack at this area.

Although the values of the Paris constants are scattered (Table 2), the main area of the graphs presented in Figure 9, show a relative agreement among the various curves.

Table 2 Five Cold Rolled Specimens Test Results

Spec. No.	K_{max}	K_{min}	Crack Dir.	Paris constants	
				C	α
1	40.00	14.99	CPR*	$4.07*10^{-9}$	1.45
2	32.50	10.50	CAR**	$9.19*10^{-10}$	1.85
3	-***	11.10	CPR	$9.82*10^{-12}$	3.19
4	44.80	9.77	CAR	$3.79*10^{-9}$	1.54
5	41.90	10.70	CPR	$5.36*10^{-16}$	6.55

*CPR= Crack perpendicular to rolling; **CAR= Crack along rolling, *** Stopped before failure.

Following the tests performed on cold rolled Ti-6Al-4V specimens, similar tests were performed on specimens produced the AM technique. As described earlier, the specimens were produced in two different directions, X-Y plane and X-Z plane, as depicted in Figure 2. At the first stage of the study, tests were performed on crack propagation of specimens produced in the X-Y plane directions and their results are presented in Figure 10 and Table 3.

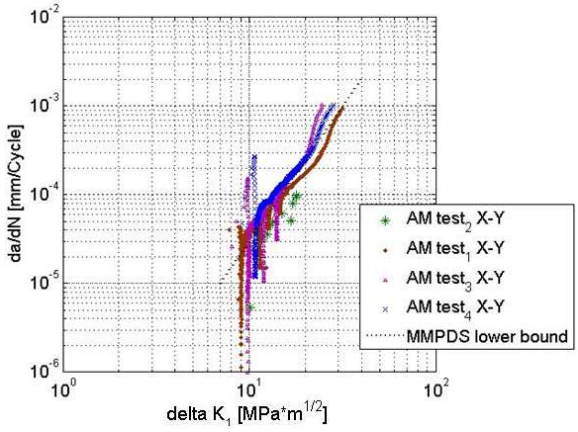

Fig. 10 Four AM Specimens Printed in the x-y Plane Direction.

Based on the test results performed on samples produced using the AM method in the X-Y plane

direction, it turned out that similar and even better results were obtained for the AM specimens in comparison with the cold rolled ones. Although the macro photos display a different picture for the AM specimens in comparison with the cold rolled ones, the micro photos clearly show similar surfaces both at the fatigue and crack areas with a micro structure being similar to pictures presented in [11, 12 and 15].

Table 3 AM Specimens Test Results

Spec. No.	K_{max}	K_{min}	Crack Dir.	Paris constants	
				C	α
AM1	31.50	8.70	X-Y	$2.15*10^{-10}$	2.27
AM2*	-	-	X-Y	$4.33*10^{-11}$	2.67
AM3	24.50	8.10	X-Y	$5.97*10^{-11}$	2.83
AM4	28.25	10.70	X-Y	$1.87*10^{-10}$	2.41
AM5	27.74	9.70	X-Y	$4.78*10^{-10}$	1.98
AM6	35.50	10.80	X-Z	$5.05*10^{-12}$	3.46
AM7	34.00	10.30	X-Z	$5.66*10^{-10}$	1.84
AM8**	29.40	9.10	X-Y	$1.79*10^{-11}$	3.22
AM9**	37.50	9.50	X-Y	$2.69*10^{-11}$	2.84

*The results are based only on a few data points manually written. The data file was found to becorrupted.
**These specimens passed a HIP heat treatment.

A further analysis of the tests performed on specimens produced using the AM method in the X-Y plane direction revealed a phenomenon which was not encountered with the cold rolled ones. This phenomenon deals with crack propagation reduction and it is clearly presented in Figures 11a-b.

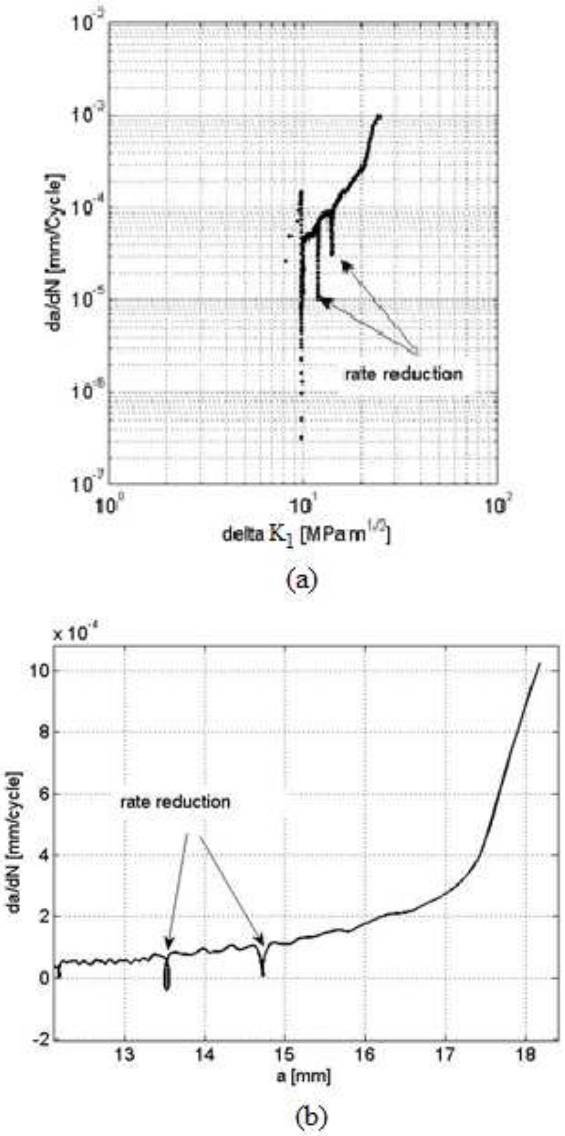

Fig. 11 Rate Reduction in AM Specimens:
(a) da/dN vs. ΔK_1; (b) da/dN vs. a.

The phenomenon is even more distinct in the micro structures photos presented in Figure 12. One can see clearly two points at which the direction of the crack propagation was changed, leading to a reduction in the crack propagation rate. The reason for this change is still not clear, although the phenomenon was noticed in all the tested specimens.

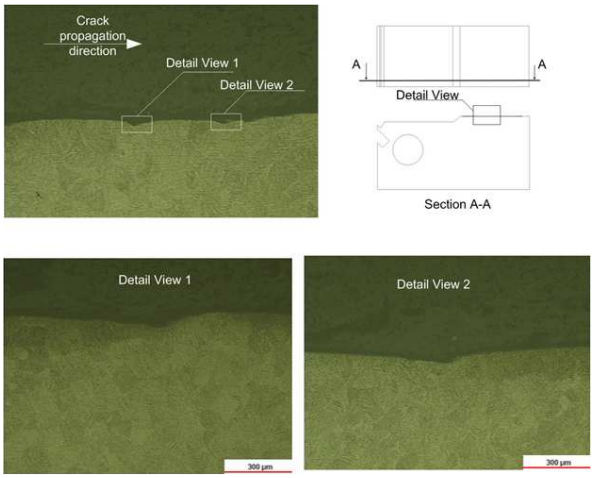

Fig. 12 Rate Reduction in AM Specimens:
(a) da/dN vs. ΔK_1; (b) da/dN vs. a.

To check the effect of the AM production direction, two additional specimens manufactured by the AM method in the direction of X-Z plane (see Figure 2) were further tested and their results are presented in Figure 13 and in Table 3, rows 6 and 7.

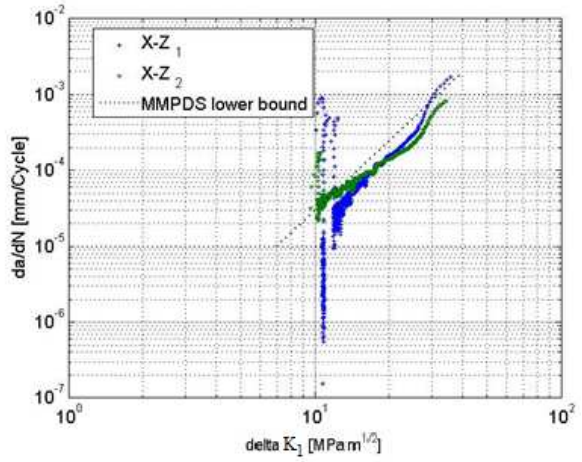

Fig. 13 Results For 2 AM Specimens Produced in the X-Z Plane Direction

To check the effectivity of the HIP heat treatment method, two specimens produced by the AM method in the direction of the X-Y plane were tested and the test results are shown in Figure 14 and Table 3, rows 8 and 9.

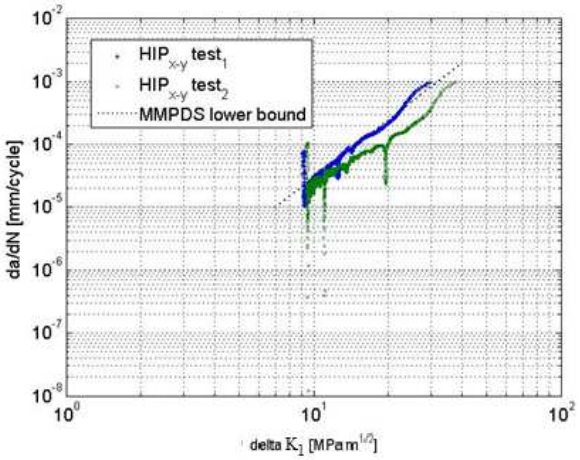

Fig. 14 Results for 2 AM Specimens Produced in X-Y Plane Direction After Undergoing the HIP Heat Treatment Process.

2.5 Lattice structures test results

The tests on the two configurations of the lattice type structures, the pols and the pits structures were performed with loads ranging 50÷500 N. Since it is not possible to attach a crack propagation gage due to the lack of an adequate surface to attach it, the crack length was measures using only the COD device. Figure 15 displays the stiffness of the two lattice structures, the pits and poles, as a function of the number of cycles. It is clear that the pits structure is superior to the poles structure, regarding both stiffness and maximal number of cycles it can sustain.

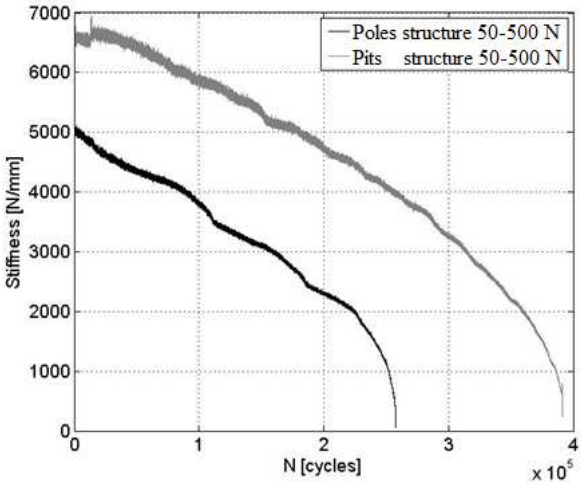

Fig. 15 Poles and Pits Specimen Stiffness vs. Number of Applied Cycles

Figures 16a-d present microscope photos taken at different magnifications for both the

poles and pits lattice structures. From Figures 16a-b it is evident that the failure in the poles structure took place at the connection among the columns, while the for the pits structure the failure was in the middle of the element with the intersections between the connecting elements remained unharmed. These findings strengthened the prediction made before, that the pits structure will be more tolerant to fatigue than the poles one.

3 Summary and conclusions

Crack propagation properties of Ti-6Al-4V alloy manufactured by laser additive manufacturing method have been evaluated and compared with results obtained from cold rolled samples machined from the same alloy ¾" plate. A good compatibility was found between the AM samples and the machined ones.

It was found that the manufacturing directions, in the case of AM method do not show any preference, yielding similar results for both the X-Y and X-Z production directions.

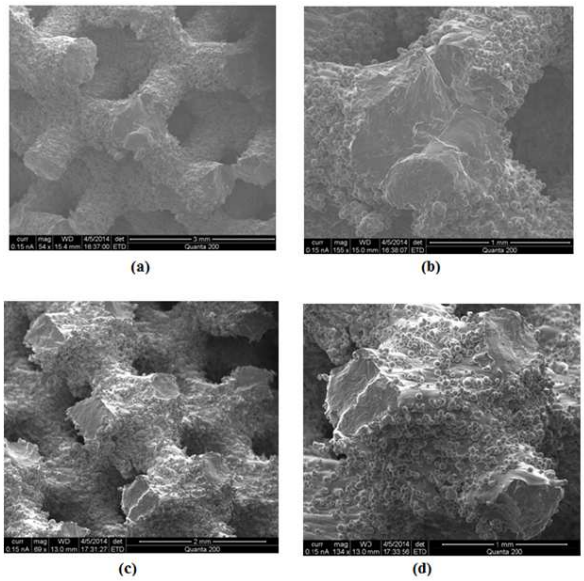

Fig. 16 Figure 20- (a) Lattice Poles Structure After Failure x54; (b) Lattice Poles Structure After Failure x155; (c) Lattice Pits Structure After Failure x69; (d) Lattice Pits Structure After Failure x134.

The application of heat treatment, like HIP heat treatment, on the AM produced samples does not seem to influence their crack propagation properties.

A crack rate reduction phenomenon was found for all the tested AM samples, still without a sound explanation. This should be further investigated.

Lattice structures, as a way of reducing weight, and yet presenting relative tolerance to fatigue had been tested and two typical structures were proposed and tested. The preliminary results are encouraging and more tests should be performed before reaching final conclusions.

References

[1] Seifi M, Dahar M, Aman R, Harrysson O., Beuth J and Lewandowski J J. Evaluation of Orientation Dependence of Fracture Toughness and Fatigue Crack Propagation Behavior of As-Deposited ARCAM EBM Ti-6Al-4V. The Minerals, Metals & Materials Society, Vol. 67, No. 3, pp. 597-607,2015.

[2] Kobryn P A and Semiatin S L. Mechanical Properties of Laser-Deposited Ti-6Al-4V. Air Force Research Laboratory, AFRL/MLLMP,Wright-Patterson Air Force Base, OH 45433-7817, 2001.

[3] Bass B S. Validating the Arcam EBM Process as an Alternative Fabrication Method for Titanium-6Al-4V Alloys. M.Sc. Thesis in Materials Science and Engineering, North Carolina State University, Raleigh, North Carolina, USA, 2007.

[4] Alcisto J, Enriquez A, Garcia H, Hinkson S, Steelman T, Silverman E, Valdovino P, Gigerenzer H, Foyos J, Ogren J, Dorey J, Karg K, McDonald T and Es-Said O S. Tensile Properties and Microstructures of Laser-Formed Ti-6Al-4V. Journal of Materials and Performance, Vol. 20, No. 2, pp. pp 203-212, 2011.

[5] Anderson T L. Fracture Mechanics Fundamentals and Applications. 3rd edition, Taylor and Francis Group, 2005.

[6] Irwin G R. Linear Fracture Mechanics, Fracture Transition, and Fracture Control. Engineering Fracture Mechanics, Vol.1 No. 2, pp. 241-257, 1968.

[7] Inglis C E. Stresses in a Plate due to the Presence of Cracks and Sharp Corners. Trans. Inst. Nav. Arch., Vol. 55, pp. 219-230, 1913.

[8] Hull C W. Apparatus for Production of Three-dimensional Objects by Steriolithography. US patent No. 4,575,330 Arcadia, CA, Mar. 11, 1986.

[9] Housholder R F. Molding Process. US Patent No. 4,247,508, Arlington, TX, Jan. 27, 1981.

[10] Griffith A A. The Phenomena of Rupture and Flow in Solids. Philosophical Transactions of the Royal

Society of London. Series A, Vol. 221, pp 163-198, 1921.

[11] Deckard, Carl R. Method and Apparatus for Producing Parts By Selective Sinturing. 4,863,538 Austin, TX, 1989.

[12] Das S, Wohlert M, Beaman, J J and Bourell D L. Processing of Titanium Net Shaped by SLS/HIP. Materials and Design Vol. 20, Nos. 2-3, pp. 115-121, 1999.

[13] Braithwaite J. On the Fatigue and Consequent Fracture of Metals. Minutes of the Proceedings of the Institution of Civil Engineers, Vol. 13, Issue 1854, Session 1853-1854, pp. 463-467, 1984.

[14] Blackwell P L and Wisbey A. Laser-aided Manufacturing Technology; Their Application to Near-net Shape Forming of a High-strength Titanium Alloy. Journal of Material Processing Technology, Vol. 170, pp. 268-276, 2005.

[15] Stuhrke W F and Carpenter J L Jr. Fracture Toughness Testing Data - A Technology Survey. NASA CR-134752, Martin Marietta Aerospace Orlando, Florida 32805, prepared for NASA Lewis Research Center, Aerospace Safety Research and Data Institute, Cleveland, Ohio 44135, USA, January 1975.

[16] Rice J R. A Path Independent Integral and the Approximate Analysis of Strain Concentration by Notches and Cracks. 1968, Journal of Applied Mechanics, Vol. 35, pp 379-386, 1968.

[17] Pugno N, M. Ciavarella M, Cornetti P Carpinteri A. A generalized Paris' law for fatigue crack growth. Journal of the Mechanics and Physics of Solids, Vol. 54, pp. 1333-1349, 2006.

[18] Pederson R. Microstructure and Phase Transformation of Ti-6Al-4V. Licentiate Thesis: Department of Applied Physics and Mechanical Engineering, Devision of Engineering Materials, Luleå University of Technology, Luleå, Sweden, 2002.

[19] Paris, P. C, Gomez M P and Anderson W E. A Rational Analytic Theory of Fatigue. The Trend in Engineering, Vol. 13, No. 1, pp 9-14, 1961.

[20] Paris, P C and Erdogan F. A Critical Analysis of Crack Propagation Laws. Trans. Of ASME, Journal of Basic Engineering, Vol. 85, No. 4, pp. 528-534, 1963.

[21] Wycisk E, Solbach A, Siddique S, Herzog D, Frank Walther F and Emmelmann C. Effects of Defects in Laser Additive Manufactured Ti-6Al-4V on Fatigue Properties. Physics Procedia, Vol. 56, pp. 371-378, 2014.

[22] Standard Test Methods for Plane-Strain Fracture Toughness of Metallic Materials. ASTM E399. 100 Barr Harbor Dr., West Conshohocken, PA 19428, USA, 1990.

[23] Standard Practice for Conducting Force Controlled Constant Amplitude Axial Fatigue Tests of Metallic Materials. ASTM E466. 100 Barr Harbor Dr., West Conshohocken, PA 19428, USA, 1996.

[24] Standard Test Methods for Tension Testing of Metallic Materials. ASTM E8/E8M. 100 Barr Harbor Dr., West Conshohocken, PA 19428, USA, 2009.

[25] Standard Test Methods for Measurement of Fatigue Crack Growth Rates. ASTM E647. 100 Barr Harbor Dr., West Conshohocken, PA 19428, USA, 1999.

[26] Rice, R C, Jackson J L, Bakuckas J and Thompson S. Metallic Materials Properties Development and Standardization (MMPDS). DOT/FAA/AR-MMPDS-01, Office of Aviation Research Washington, D.C. 20591, U.S. Department of Transportation, Federal Aviation Administration, Office of Aviation Research, January 2003.

4 Contact Author Email Address

mailto:haim@technion.ac.il

Copyright Statement

INVESTIGATION OF CRACK PROPAGATION PROPERTIES OF ADDITIVE MANUFACTURING PRODUCTS